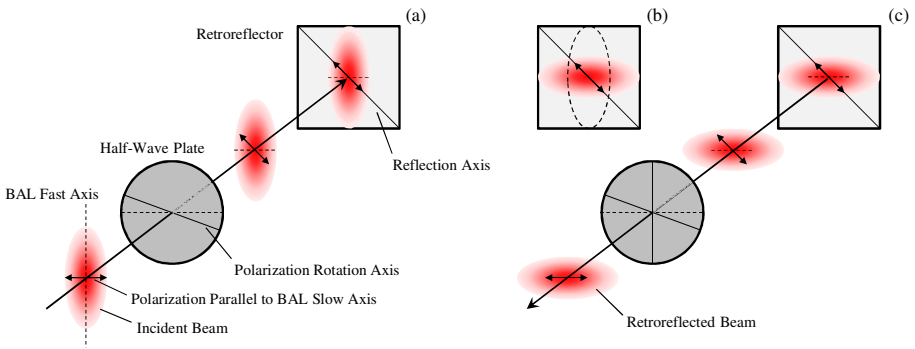

Fig. 2. Diagram illustrating mode swapping with retroreflector. (a) For maximum feedback the half-wave plate rotates the TE polarization of the incident beam to be parallel with the reflection axis of the retroreflector. (b) The beam reflects across the reflection axis of the retroreflector swapping the fast- and slow-axis spatial modes present in the incident beam. Since the polarization is parallel to the reflection axis, it remains unchanged after retroreflection. (c) The retroreflected beam passes back through the half-wave plate where the polarization is rotated back parallel to the TE polarization amplified by the laser diodes. The beam is depicted as astigmatic for clarity, but a stigmatic beam maximizes coupling of the retroreflected beam back into the fast- and slow-axis facets of the BAL emitters.

output powers measured here, at higher powers TM polarized light could cause excess heating in the BAL emitters and degrade the array's performance. This potential problem can be easily mitigated with an optimized grating or an additional polarizing beam splitter placed between the grating and the half-wave plate.

The retroreflector uses an off-axis reflection to provide feedback via the loop mirror. The off-axis implementation is used to prevent beam distortions in the retroreflected beam. When the incident beam is centered on the reflection axis, distortion is evident, as shown in Fig. 3(a). This can be compared with Fig. 3(b), showing an image of the beam reflected off-axis which looks nearly identical to the incident beam, shown in Fig. 3(c) for reference. For an on-axis reflection, interference between the two sides of the incident beam causes the distortion. The two sides of the retroreflector are not at exactly 90° (angular tolerance is specified as ± 2 arcseconds, equal to ± 0.01 mrad), and the two beams walk across each other after reflection.

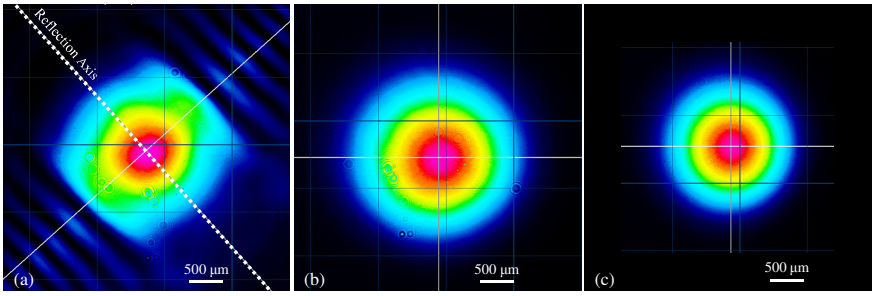

Fig. 3. Characterization of aberrations from the retroreflector. The highest and lowest intensities are shown magenta and black, respectively. Images were taken of a retroreflected HeNe beam with the incident beam centered (a) directly on the retroreflector's reflection axis and (b) far away from the reflection axis. (c) Image of the incident HeNe beam used to test the retroreflector. The beam distortion in (a) is due to interference between the two sides of the reflected beam. The two sides walk across each other due to the imperfect 90° angle between the two reflecting surfaces.

3. Results and discussion

Optical spectra, power, and beam quality were measured for all three WBC cavity configurations. Together, these measured quantities are used to compare the brightness

#191385 - $15.00 USD Received 29 May 2013; accepted 1 Jul 2013; published 18 Jul 2013

achieved for each configuration. In the mode-imaging cavity, the distance between the lenses used in the 1.5:1 slow-axis telescope is re-optimized for output powers greater than 1 W (currents > 8 A). Increasing the separation between the telescope lenses with larger drive currents optimized the output power and beam quality. The optimal separation increased monotonically over the range of currents investigated, reaching a maximum of 8 mm at 11 A and 1.62 W output power. The behavior suggests the formation of a thermal lens within the BAL emitters [21] and increased overlap of higher order modes with the gain profile within the emitters relative to overlap of the fundamental mode.

An output spectrum from the mode-imaging WBC cavity is shown in Fig. 4(a). The spectrum shows multiple individual emission peaks within a bandwidth of about 25 nm. Each emission peak is produced from one emitter in the array. The center wavelength of each peak is determined by the array pitch and cavity optics, and depends on the incident and diffraction angle of the beam from each emitter relative to the grating [20]. The output spectra for all three laser configurations are nearly identical.

The L-I characteristics for all three laser cavity configurations are shown in Fig. 4(b). The threshold current and slope efficiency are 4.1 A and 0.42 W/A, respectively, for the standard Littman-Metcalf WBC cavity without any mode filtering. The threshold currents for both the standard cavity with intracavity mode filtering and the mode-imaging cavity are similar, and the slope efficiencies are nearly identical at 0.26 W/A and 0.24 W/A, respectively. The standard cavity with the intracavity mode filter did not generate output powers beyond 1.02 W even for currents above 8.5 A. This corresponds to the same current where optimization of the slow-axis telescope becomes necessary in the mode-imaging cavity. Thermal lens formation within the BAL emitters may cause reduced transmission through the intracavity slit. Additionally, the anti-reflection coating on the BAL array is imperfect, and drive currents of ~10 A correspond to chip-mode lasing without an external cavity. At 8.5 A, the gain in the fundamental external cavity mode may become equal to the gain of the higher-order chip modes. Further increasing the current would increase the relative gain for the chip modes and thus cause a reduction in the observed power in the fundamental mode circulating within the external cavity.

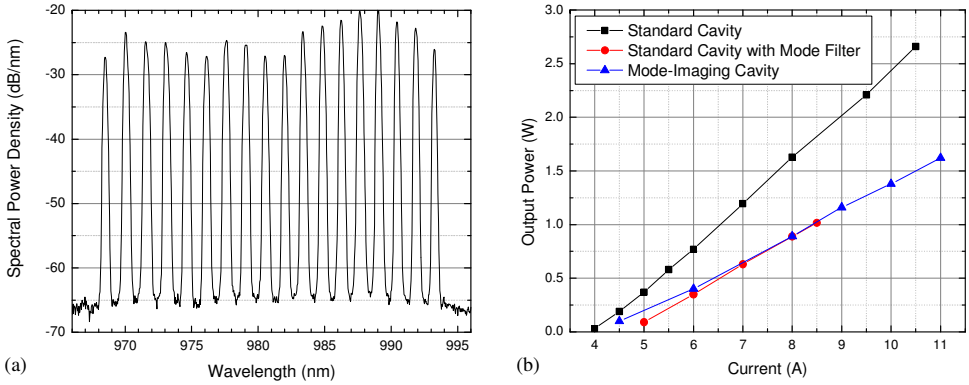

Fig. 4. (a) Spectrum from the mode-imaging cavity taken at a drive current of 9 A producing 1.16 W of output power. The spectrum is typical of all the wavelength beam combined (WBC) laser cavities investigated. Each emission peak corresponds to one emitter in the array with center wavelengths determined by the particular incident and first-order diffraction angle from the grating. The centroid of the spectrum is at 983 nm. (b) L-I curves for the standard WBC cavity without (black squares) and with (red circles) a 130-μm wide intracavity slit used for mode filtering and for the mode-imaging cavity (blue upward pointing triangles).

The beam quality is determined by focusing the beam reflected from the uncoated 3° wedge with a 100-mm focal length achromatic doublet lens and measuring the fast- and slow-axis beam waists with a CMOS camera at several positions. The measured fast- and slow-axis beam caustics were fit using the standard hyperbolic equation [22] with the minimum waist, the axial position corresponding to the minimum waist, and the M^2 factor as free parameters.

#191385 - $15.00 USD Received 29 May 2013; accepted 1 Jul 2013; published 18 Jul 2013

The fast-axis M^2 values range from 1.2 to 1.4 for all cavity configurations, and the measured slow-axis beam quality as a function of output power for all three cavity configurations is shown in Fig. 5(a). The slow-axis M^2 increases with output power for all cavity configurations. Both the standard WBC cavity with mode filter (red circles) and the mode-imaging cavity (blue triangles) show dramatic improvement in beam quality over the standard cavity with no mode filtering. While both cavity configurations show similar trends for the measured slow-axis M^2 values, the standard cavity with slow-axis mode filtering could not generate output powers beyond ~1 W. However, the mode-imaging cavity data shows that the M^2 values remain low until an output power of 1.16 W is reached, after which the beam quality quickly degrades. The drive current corresponding to these transitions coincides closely with the threshold current for lasing observed for the BAL array without any external cavity feedback. Improving the anti-reflection coating on the front facet of the diodes or angle cleaving the laser facets should permit higher powers to be reached before observing substantial degradation in the beam quality.

The radiance or brightness, B, of the WBC lasers is given by [17],

$$B = \frac{P}{\lambda^2 M_x^2 M_y^2}, \tag{1}$$

where P is the output power, λ is the center wavelength, and M_x^2 and M_y^2 are the slow- and fast-axis M^2 values. Brightness computed using Eq. (1) as a function of total output power for all three cavity configurations is shown in Fig. 5(b). Again, the standard cavity with mode filtering and the mode-imaging cavity are seen to have similar brightness for output powers up to ~1 W, reaching peak values in excess of 45 $MW \cdot cm^{-2} \cdot sr^{-1}$, approximately a factor of two more than that of the standard cavity without mode filtering at the same output power. The brightness for the mode-imaging cavity is seen to degrade at output powers beyond 1.16 W as a direct consequence of the rapid increase in the slow-axis M^2 values.

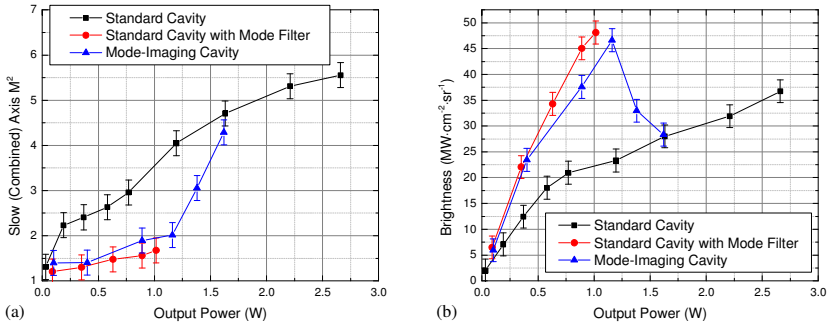

Fig. 5. (a) Average slow-axis beam quality as a function of output power for the standard wavelength beam combined (WBC) cavity without (black squares) and with (red circles) intracavity mode filtering and for the mode-imaging cavity (blue upward pointing triangles). Slow-axis M^2 values for both the standard cavity employing mode filtering and the mode-imaging cavities are improved over the standard cavity without mode filtering, and follow very similar trends with the notable exception that the standard cavity with mode filtering could not generate output powers beyond ~1 W. (b) Average brightness as a function of output power for all three cavity configurations. The standard WBC cavity employing mode filtering (red circles) and the mode-imaging cavity (blue upward pointing triangles) show maximum brightnesses of greater than 45 $MW \cdot cm^{-2} \cdot sr^{-1}$. Error bars indicate ± one standard deviation from multiple measurements as determined from the cavity configuration with the highest measured standard deviation.

4. Conclusion

A novel technique to dramatically improve beam quality produced from BALs in which the emitted fast-axis mode is reimaged back onto the slow-axis dimension of the laser facet has

#191385 - $15.00 USD Received 29 May 2013; accepted 1 Jul 2013; published 18 Jul 2013

been demonstrated. Together, the fast-axis lens and BAL facets function as optical Fourier filters, suppressing lasing of higher-order transverse modes within the external cavity. The technique is simple and broadly applicable to BAL single emitters and arrays employing external cavity feedback, including both coherent and wavelength beam combined systems. Slow-axis M^2 values of ≤ 2 at output powers up to 1.16 W have been achieved from a BAL array in a WBC cavity employing this mode-imaging technique, producing a maximum brightness of 47 $MW \cdot cm^{-2} \cdot sr^{-1}$ at a center wavelength of 983 nm. The beam quality improvement from the mode-imaging cavity configuration closely parallels that observed from a standard WBC cavity employing a slow-axis telescope and slit as an optical Fourier filter due to filtering characteristics of the mode-imaging cavity. To the authors' knowledge, this work represents the first application of intracavity Fourier filtering to an array of single-stripe BAL emitters, with demonstrated output powers and brightnesses in excess of those reported for the near single mode emitters within the multi-stripe array used in [13].

Both intracavity Fourier filtering and the newly demonstrated mode-imaging technique have been demonstrated to improve the beam quality from a BAL array within a WBC setup. The mode-imaging technique achieved ~20% higher output power compared with the mode filter cavity before significant beam quality degradation was observed. Simplifying the mode-imaging cavity setup by employing fewer optical components may further increase the maximum output power and brightness. For example, utilizing matched fast- and slow-axis collimating lenses which produce astigmatic beams directly from the emitters would allow the secondary fast-axis collimating lens and the two slow-axis telescope lenses to be removed from the current setup. Fewer optics and better fast- and slow-axis mode matching would reduce intracavity losses, provide simpler and more robust cavity alignment, and allow much shorter cavity lengths to be realized. At high powers, competition from chip-mode lasing is expected to spoil the beam quality. Increasing the lasing threshold of the BAL array through better anti-reflection coatings or utilizing emitters with angled facets should increase the usable output power and maximum brightness.

Acknowledgments

This work is supported by the Air Force Office of Scientific Research (AFOSR) under grant number FA9550-11-1-0026 through the Young Investigator Program.

#191385 - $15.00 USD Received 29 May 2013; accepted 1 Jul 2013; published 18 Jul 2013